Vibrational Circular Dichroism study of chiral food additives: γ-valero- and γ-caprolactone

M. Sánchez Valera[1], R. Casas Jaraíces[1], M. Montejo[1] and P. G. Rodríguez Ortega[2]*
[1]*Department of Physical and Analytical Chemistry, Experimental Sciences Faculty, University of Jaen, E-23071, Jaén, Spain*
[2]*Department of Specific Didactics, Educational Sciences Faculty, University of Cordoba, E-14071, Córdoba, Spain*
*Corresponding author: mrodriguez1@uco.es

Abstract

γ-valerolactone and γ-caprolactone are commonly used as flavor additives in the food industry. In the present work we fully explore the molecular structure and conformational distribution of enantiopure γ-valerolactone and γ-caprolactone in solution state by using Vibrational Circular Dichroism (VCD) spectroscopy assisted by quantum chemical calculations. In order to establish the most accurate DFT method for this type of samples a set of methods and basis sets have been implemented and their performances have been compared. Subsequently, we have performed a complete vibrational assignment, which allowed to detect certain key vibrational features related to specific solution-state conformational speciation. In spite of the rigidity of the samples being studied, our results point to the incidence of conformational mixture in CCl_4 solution in both samples.

1. Introduction

Chirality is ubiquitous in nature and, thereforemany biological processes are sensitive to chirality.[1] For example, human senses such as taste and smell are primarily enantioselective [2], so commonly the reaction triggered by our receptors (both smell and taste) depends on the specific configuration of the interacting molecules in our receptors. Many chiral odorants are used in the food industry. Sometimes, these are natural products, which enantiomeric composition is known and used to elucidate if ingredients found in the foods have undergone particular synthetic processes to produce artificial substances (i.e., identify irregular adulterations during the fabrication process)[3],[4], to regulate the authenticity of the natural chiral flavors used as ingredients, to analyze the quality of the foods [5], as well as establishing their geographical origin. [6]

The flavor (aroma and taste) of a substance is the result of a synergistic organic reaction to a combination of a group of molecules typically among which are γ-lactones. The title species, namely, γ-valerolactone and γ-caprolactone (Figure 1a and 1b, respectively) are butan-4-olide derivatives either methyl or ethyl substituted in C_2 position [7,8].

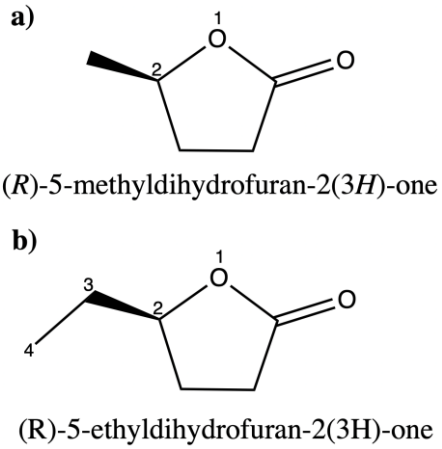

Figure 1. Molecular structure, atom numbering and systematic IUPAC name for a) (R)-γ-valerolactone and b) (R)-γ-caprolactone

These lactones can exist as two different enantiomeric forms depending on the R or S configuration at C_2, each enantiomer being characterized by a different aroma and/or aromatic intensity. Several studies have characterized the aroma components in different foods (e.g. brown sugar, molasses, nuts and fruits) that contain these lactones [9]. For these reasons, these substances are currently commonly used as flavoring and/or odorants additives not only of foodstuffs but also in cigarettes, beauty products and/or toys, among others. [10] Furthermore, the usefulness of γ-caprolactone in the food industry is enhanced by the fact that it is competent to promote the growth of bacteria with biocontrol activity against putrefaction pathogens. [11]

To the best of our knowledge, in addition to some specific vibrational studies on γ-caprolactone [12], a complete vibrational characterization of γ-valerolactone and γ-caprolactone, involving the theoretically assisted analysis of their vibrational spectra, is lacking.

Motivated by this, in this work we report the study of the molecular structure and the conformational landscape of the (R) enantiomers of γ-valerolactone and γ-caprolactone through the use of a combined experimental and theoretical approach sustained by the comprehensive analysis of their solution-phase chiral signatures in the corresponding Vibrational Circular Dichroism (VCD) spectra, which constitute the firstly reported VCD data of the samples.

In this regard, it is worth to mention that the VCD technique represents the most sensitive method of vibrational spectroscopy with direct application for enantiomeric differentiation (and absolute configuration assignment) and conformer distribution in solution state [13]. In fact, VCD-based strategies have been successfully implemented in the characterization of more complex but structurally related lactones derivatives [14].

2. Materials and methods

2.1.Computational details

Conformational searches were carried out with the GMMX module of GaussView 6.0 [15] using the MMFF94 [16] force field. This module allows scanning the potential energy surface of the studied systems by generating an arbitrary number of structures (selected by the user) obtained by giving random values to a set flexible bonds previously chosen. The user also selects the energy threshold within which the selected molecular conformations can fall.

All of the structures obtained from the conformational search were confirmed as real minima in the PES by structure optimization and harmonic vibrational frequency calculations using the following DFT-based methods: the widespread hybrid B3LYP functional [17] correlation functional, the hybrid B3PW91 functional [18], the single-hybrid PBE1PBE functional [19], the long-range corrected hybrid ωB97XD functional [20] and the highly parameterized approximate exchange-correlation energy hybrid meta-GGA M062X functional [21]. B3PW91 was implemented in combination with the Pople style basis sets (6-31G*, 6-31+G, 6-311++G**) [22], the DGDZVP basis set [23], and the Dunning-Huzinaga basis set (cc-pVDZ, cc-pVTZ, aug-cc-pVDZ and aug-cc-pVTZ) [24]; for the remaining methods only the aug-cc-pVTZ basis set was used. During the geometry optimization process, the SCF = tight and Int = Ultrafine options were used to tighten the convergence criteria. Since experimental spectra were recorded in CCl_4 solution, all calculations implemented the integral equation formalism (IEF) version of the polarizable continuum solvation model (IEF-PCM) [25] using the dielectric constant value for CCl_4 (ϵ = 2.2). All DFT calculations were performed with Gaussian16 [26].

2.2.Vibrational spectra

Enantiopure and racemic samples of γ-valerolactone and γ-caprolactone were purchased from Sigma-Aldrich and used without further purification. FTIR and VCD spectra were recorded in CCl_4 solution using a JASCO FVS-6000 FTIR spectrometer. The device is equipped with a liquid-N_2-cooled MCTV detector for measurements in the 2000–850cm^{-1} range, a high intensity ceramic infrared light source and a ZnSe Photo Elastic Modulator (PEM). For measurements, sample concentrations in CCl_4 (0.15M-0.8M) were optimized in absorbance for a Spectral-Systems super sealed cell equipped with BaF_2 windows with a pathlength of 0.075mm. The VCD and IR spectra were recorded using a spectral resolution of 4 cm^{-1} and after accumulating 40000 (VCD) and 250 (IR) scans. Baseline corrections and VCD artifacts suppression were achieved by subtracting the spectra recorded for the solutions of the racemic mixtures under the same experimental conditions (concentration, IR absorbance, resolution and accumulation time) that were used for the samples.

All reported and discussed theoretical IR and VCD spectra have been constructed by convoluting the Boltzmann-weighted spectra of individual conformers using GaussView 6.0 [15], which uses Boltzmann's populations calculated from Gibbs free energies. The theoretical-experimental match has been quantified by implementing a similarity analysis

using the CompareVOA program [27], which helped to select the theoretical method to perform the vibrational analysis and assignment.

3. Results and Discussion

3.1. Molecular structure and conformational landscape

3.1.1. (R)-γ-valerolactone

Figure 2 shows the output of the conformational search performed in this study for (R)-γ-valerolactone. Two conformers were found, the main difference between them lying on the preferred orientation adopted by the methyl group at C5 (equatorial C^{I} or axial, C^{II}). In both structures the cyclopentane ring adopts the envelope conformation, arrangement that releases the torsional tension caused by high eclipsing hydrogens that would produce a planar conformation.

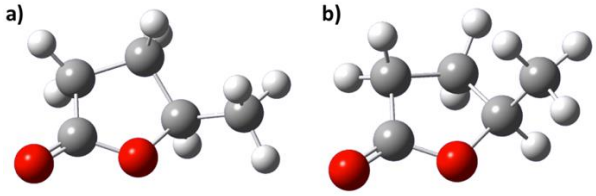

Figure 2. Optimized structures of the conformers found of γ-valerolactone at the B3LYP/aug-cc-pVTZ level a) C^{I} and b) C^{II}.

The theoretical populations of each conformer at the above-mentioned levels of theory were determined in CCl_4 from the Boltzmann equation in terms of the E_0 energies and are shown in Table 1.

Table 1. DFT/aug-cc-pVTZ relative Gibbs free energies (G; kcal/mol) and Boltzmann's populations (%) for the conformers of γ-valerolactone.

	Gas Phase		PCM (CCl_4)									
	B3LYP		B3LYP		B3W91		PBE1PBE		ωB97XD		M062x	
	ΔG	%Pop	ΔG	%Pop	ΔG	%Pop	ΔG	%Pop	ΔG	%Pop	ΔG	%Pop
C^{II}	0.84	19.4	0.81	20.3	0.79	20.1	0.76	21.6	0.51	29.8	0.54	28.7
C^{I}	0.00	80.6	0.00	79.7	0.00	79.2	0.00	78.4	0.00	70.2	0.00	71.3

All methodologies provide comparable results and all agree with the equatorial conformer as the most stable species. However, as shown, while non-dispersion-corrected methods predict a 80:20 ratio between the equatorial and axial conformers, ωB97XD and M062x methods close the energy gap by predicting a 70:30 ratio instead. These differences that, as will be shown below, do not significantly affect the calculated vibrational spectra, are must probably due to differences in the way repulsive interactions between the methyl group and the ring are accounted for.

3.1.2. (R)-γ-caprolactone

Figure 3 collects the optimized structures of the conformers found for (R)-γ-caprolactone at the B3PW91 / aug-cc-pVTZ level. In this compound, two main factors determine the conformational equilibrium: (1) the axial/equatorial arrangement of the ethyl chain and (2) the dihedral angle of the ethyl chain with respect to the O_1 atom leading to gauche ($\phi_{O1C2C3C4}$ ~ 65°) or anti ($\phi_{O1C2C3C4}$ ~ -180°) conformations (see Figure 1 for atom numbering). Hence, four conformers were found through our MM/DFT conformational search.

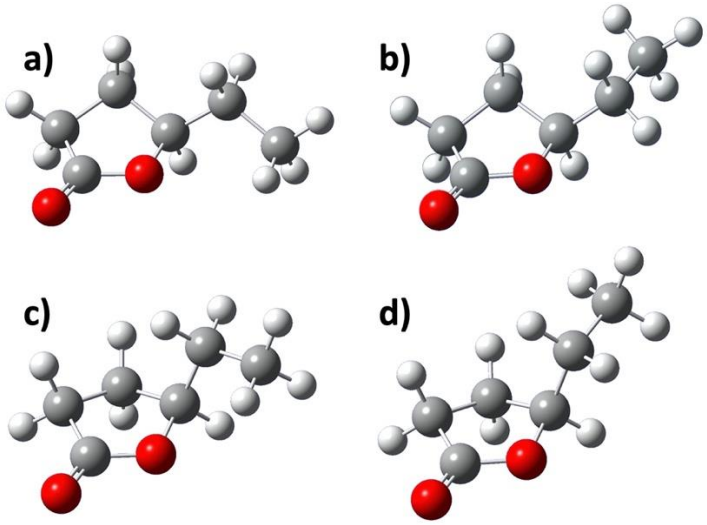

Figure 3. Optimized structures of the conformers found of γ-caprolactone at the B3LYP/aug-cc-pVTZ level. (a) C^{I}_{anti}, (b) C^{I}_{gauche}, (c) C^{II}_{anti}, (d) C^{II}_{gauche}.

The theoretical populations of these species were calculated in CCl_4 from the Boltzmann equation in terms of the Gibbs free energies for the set of reported methods and are shown in Table 2.

Table 2. DFT/aug-cc-pVTZ relative Gibbs free energies (G; kcal/mol) and Boltzmann's populations (%) for the conformers of γ-caprolactone.

	Gas Phase		PCM (CCl_4)									
	B3LYP		B3LYP		B3PW91		PBE1PBE		ωB97XD		MO62x	
	ΔG	%Pop	ΔG	%Pop	ΔG	%Pop	ΔG	%Pop	ΔG	%Pop	ΔG	%Pop
C^{II}_{anti}	0.87	12.8	0.89	11.5	0.84	12.1	0.84	12.1	0.69	12.9	0.54	15.9
C^{II}_{gauche}	1.28	6.4	1.13	7.7	1.02	9.1	1.07	8.2	0.68	13.2	0.73	11.6
C^{I}_{anti}	0.00	55.4	0.00	52.0	0.00	50.2	0.00	49.8	0.00	41.3	0.00	39.5
C^{I}_{gauche}	0.46	25.3	0.35	28.8	0.33	28.6	0.30	29.9	0.14	32.7	0.11	32.9

All theoretical approaches agree that equatorial conformers are the most stable species the *anti* configuration (C^{I}_{anti}) being the preferred orientation for the ethyl group. Nonetheless, the functionals parametrized to account for dispersion tip the balance between the gauche and *anti* forms of the equatorial conformers almost to equity. Again, the energy gap between the equatorial and the more hindered axial conformations is closed when electronic dispersion is considered, although the overall equatorial:axial ratio is barely affected by the inclusion of dispersion (from 80:20 to 75:25).

As expected, implicit solvent consideration of such a low polarity solvent hardly affects the conformational distributions calculated for (R)- γ-valerolactone and (R)- γ-caprolactone as compared with those obtained in gas phase (Tables 1 and 2).

3.2.Vibrational Analysis

Always whithin the framework of the PCM formalism (since all the spectra reported have been recorded in CCl_4 solution), the precision of a set of DFT functionals and basis sets to reproduce the IR and VCD spectra of the samples under study has been evaluated by calculating the theoretical-experimental similarity indices according to the methodology described elsewhere [27] (see Table 1S and 2S in ESI).

To assess the accuracy of the DFT methods, we have used the aug-cc-pVTZ basis set as reference (as it is the largest). As shown, the performance of the different DFT functionals used is comparable and generally good, although slightly better in the case of B3PW91 in both samples. Our result is further endorsed by the fact that B3PW91 is a widely recommended functional for VCD spectra calculation [28].

As concerns the basis set size (that has been tested using the B3PW91 functional), it can be stated that the use of TZ quality basis sets introduce an improvement in the calculated similarity indexes which is mostly appreciable in the case of the VCD spectra (see Table 2S). Nonetheless, and although the inclusion of diffuse functions is strongly recommended for computing VOA spectra (particularly in ROA calculations) and generally implies and better prediction of molecular properties, in accordance with literature data, no significant improvements are observed in our case (compare, e.g., calculated similarity values for cc-pVTZ and aug-cc-pVTZ, Table 2S). Anyhow, for being the overall best performing method (and computationally affordable given the size of the systems studied) the subsequent vibrational analysis has been made taking the PCM:B3PW91/aug-cc-pVTZ combination as reference.

3.2.1. (R)-γ-valerolactone

In order to evaluate the conformational speciation of the samples in solution, the study of the IR and VCD spectra is mainly focused in the 1500- 850 cm^{-1} region where the identification of conformer-discriminating bands is most probable. Figure 4 shows the experimentally recorded IR and VCD spectra of the sample in the region of interest.

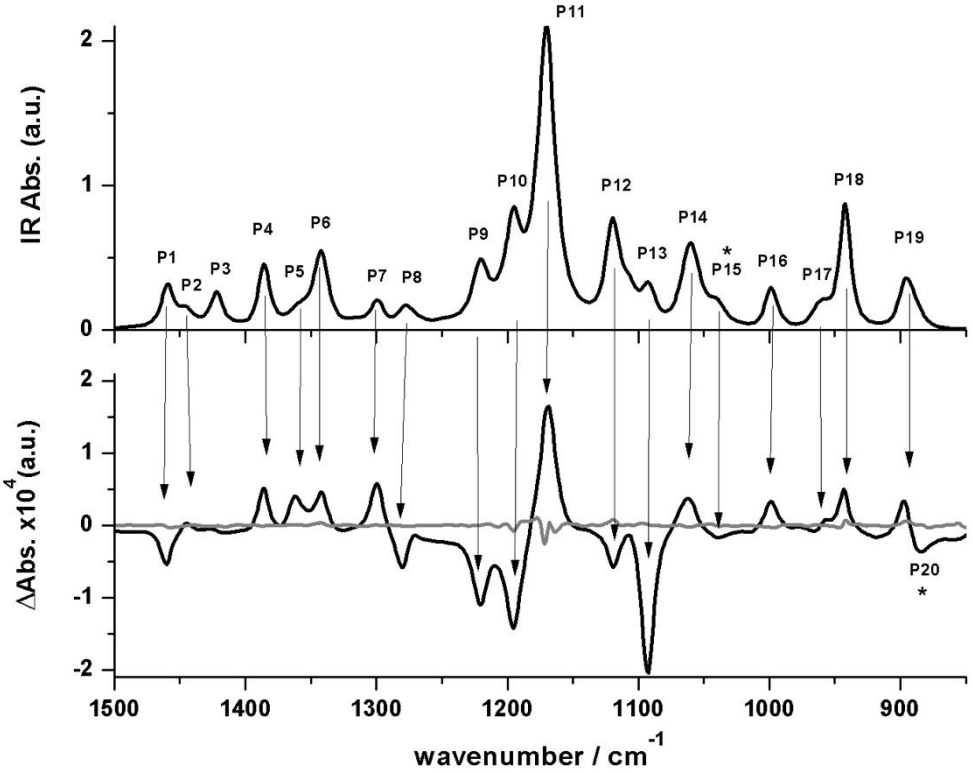

Figure 4. Experimentally recorded IR (top) and VCD (bottom) spectra in the 1500-850 cm^{-1} region for (R)-γ-valerolactone in CCl_4 solution (0.8M) and peak designation. Noise curve in grey.

Up to 20 vibrational bands, out of the total vibrational normal modes (39) of the sample, are detected in the region of interest. These are listed in Table 3 along with their proposed assignment. The overlapping spectra of all the conformers are collected in Figure 1S (ESI).

As reported, the vast majority of the vibrational bands can be assigned to normal modes calculated for the C^{I} (equatorial) conformer, which is by far the most populated (it is present in the sample in a 4:1 ratio with respect to the axial conformer, Table 1). This fact, together with the coincidence in the wavenumbers calculated for the normal modes of the two conformers, has not prevented, however, obtaining subtle but consistent evidence of the incidence of conformational mixture in the sample.

Table 3. Assignment of the experimental IR and VCD bands in the 0.8M CCl_4 solutions of (R)-γ-valerolactone.

	Experimental (cm^{-1})		Theoretical[1]						Assignment[5]
			C^{I}			C^{II}			
	IR	VCD	Scaled[2]	IR int.[3]	R_i[4]	Scaled[2]	IR int.[3]	R_i[4]	
P20	-	(-)884				885	21	-69	$twCH_2 + \rho CH_3$
P19	895	(+)897	893	22	34				$twCH_2 + \rho CH_3$
P18	942	(+)947	943	53	15	939	17	17	$waCH_2$
P17	960(sh)	(+)955	950	17	27	960	26	-19	$\rho\, CH_2 + \rho\, CH_3$
P16	989	(+)999	998	9	15	1000	29	20	$v\, CC + waCH_2$
P15	1041(sh)	(-)1037				1039	42	-21	$waCH_2 + waCH_3$

P14	1060	(+)1061	1063	65	51				ρCH_2
P13	1092	(-)1092	1090	18	-75	1085	18	-62	$\rho CH_2 + \rho CH_3$
P12	1119	(-)1119	1121	76	-13				$\rho CH_2 + \rho CH_3$
						1107	64	31	
P11	1170	(+)1168	1169	155	99	1169	260	70	$vCC + vCO$
P10	1195	(-)1196	1193	102	-73				$twCH_2 + waCH_3$
						1182	8	-37	
P9	1221	(-)1221	1222	27	-41				$twCH_2 + \rho CH_2$
						1214	16	0	
P8	1278	(-)1280	1281	7	-28	1277	22	51	$waCH_2$
P7	1300	(+)1300	1300	18	27	1306	3	10	$scCH_2$
P6	1342	(+)1342	1344	31	0	1344	41	28	δCH
P5	1362(sh)	(+)1362	1365	2	9	1362	12	17	$scCH_3$
P4	1386	(+)1382	1386	29	20	1381	20	6	ρCH_3
P3	1421	-	1426	10	0	1428	9	-3	$scCH_3$
P2	1445	(+)1437	1449	5	6	1449	5	3	$scCH_3$
P1	1459	(-)1460	1460	5	1	1459	7	-8	$scCH_2$
			1463	8	-10	1466	6	-4	$scCH_2$

[1]B3PW91/ aug-cc-pVTZ level (PCM).[2]The scale factor=0.982 was optimized to maximize the similarity between the experimental and theoretical IR and VCD profiles according to the methodology reported elsewhere [27]; [3]Calculated IR intensities in km/mol; [4]Calculated VCD rotational strengths (Rix10^{-44}) in esu^{2}cm^2; [5] Tentative description based in the visual inspection of the vibrational motions using Gaussview6; Symbols: ν =stretching, ρ =rocking, tw=twisting, wa=wagging, sc= scissoring; δ=deformation.

For instance, the so-called P20 is a negative peak that is observed in the VCD spectra (part of a +/- couplet) with no apparent counterpart in the IR spectrum, where the so-called P19 is observed and assigned (along with the corresponding positive VCD band) to the equatorial conformer. As shown in Table 3, P20 is attributable to the axial conformer for which a strong negative band is expected to appear in this region accounting for the twisting and rocking of methylene (cycle) and methyl groups.

Furthermore, the so-called P15 (shoulder at 1041 cm^{-1} in the IR spectrum, subtle negative band at 1037cm^{-1} in the VCD spectrum) can be assigned to the wagging of the methyl and methylene (cycle) groups of the axial conformer according to its calculated value.

As concerns the validity of the calculation method chosen (PCM: B3PW91/ aug-cc-PVTZ), the theoretical spectra at this level have been built by convoluting the Boltzmann weighted individual spectra of the axial and equatorial conformers. As shown in Figure 5, the reproduction of the experimental spectra its outstanding with just slight differences in the calculated intensities of the bands around 1350 cm^{-1} in the VCD spectrum.

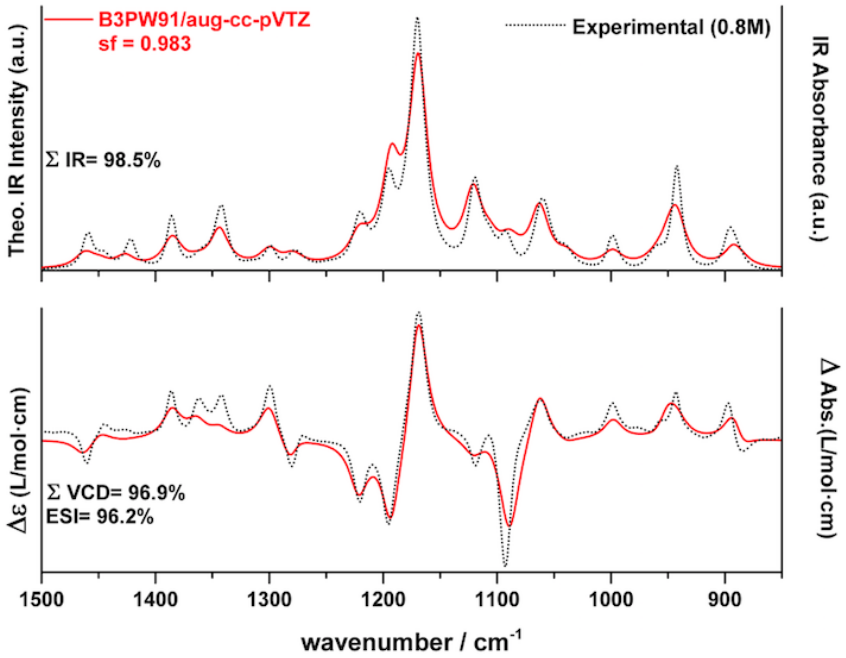

Figure 5. Theoretical-experimental comparison of the IR (above) and VCD (below) spectra of (R)- γ-valerolactone in CCl_4 solution (0.8M).

In fact, the goodness of our theoretical model is evidenced by the results of the statistical validation performed by the CompareVOA software with neighborhood similarity indexes of 98.5% and 96.9% calculated, respectively, for the match between the experimental and theoretical IR and VCD profiles.

It is worth mentioning that the remaining methods also reproduce successfully the experimental observations (see Table 1S and Figure 1S in the ESI). Although the results with all the methods are comparable, the previously commented choice of B3PW91 is based on two facts: (i) higher similarity indices; (ii) the subtlety of the signatures of the axial conformer in the experimental profile make more reliable the 4:1 equatorial/axial proportion predicted by this method than the ca. 2:1 proportion predicted by dispersion corrected methods, that maybe underestimate the equatorial/axial energy difference.

3.2.2. (R)-γ-caprolactone

Figure 6 displays the experimentally recorded IR and VCD spectra, that show more bands, wider and with more complex shapes than in the case of (R)-γ-valerolactone, promptly revealing that the presence of several conformers in the sample is plausible.

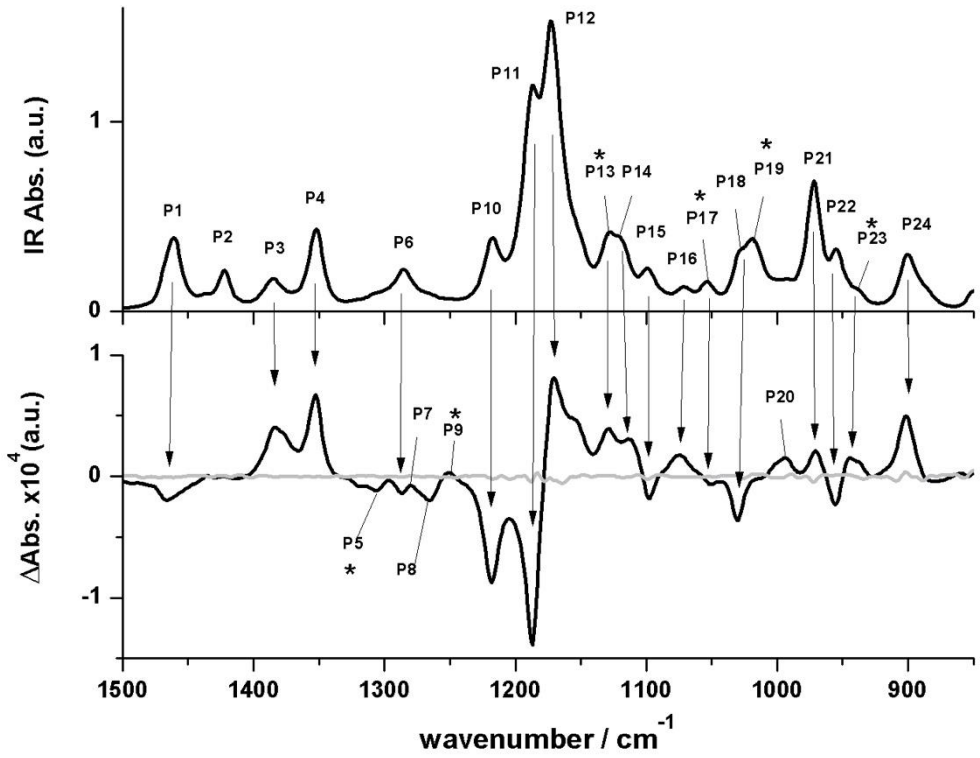

Figure 6. Experimentally recorded IR (top) and VCD (bottom) spectra in the 1500-850 cm^{-1} region for (R)-γ-caprolactone in CCl_4 solution (0.8M) and peak designation. Noise curve in grey.

In this case, taking together the IR and VCD spectra, 24 different spectral features are observed. As reported in Table 4, all of them have been assigned to vibrational normal modes of the sample, in agreement with their calculated values. Overlapping spectra of all the conformers are collected in Figure 3S (ESI).

Table 4. Assignment of the experimental IR and VCD bands in the 0.8M CCl_4 solutions of (R)-γ-caprolactone.

	Experimental (cm^{-1})		Theoretical[1]												Assignment[5]
			C^I anti			C^I gauche			C^{II} anti			C^{II} gauche			
	IR	VCD	Scaled[2]	IR int.[3]	R_i[4]	Scaled[2]	IR int.[3]	R_i[4]	Scaled[2]	IR int.[3]	R_i[4]	Scaled[2]	IR int.[3]	R_i[4]	
									886	18	-17	886	25	-51	$\rho CH_{2(r)} + waCH_3$
P24	900	(+)901	903	24	53	901	37	47							$\rho CH_{2(r)} + waCH_3$
P23	944(sh)	(+)944				941	11	28				937	10	4	$waCH_3 + waCH_{2(e)}$
P22	955	(-)955	951	25	-24				956	27	-17				$waCH_3 + waCH_{2(e)}$
P21	972	(+)971	972	69	22	976	22	-10	972	66	5	976	17	10	$waCH_3 + waCH_{2(e)}$
P20		(+)994	991	10	17	1000	7	18	989	6	-20	1003	11	-30	$waCH_{2(r)} + vCC$
P19	1019											1016	102	13	$vCO + waCH_3$
P18	1028	(-)1030	1030	22	-36	1026	92	9	1031	30	12				$vCO + waCH_3$
P17	1054	(-)1054				1056	28	16	1051	16	-53	1050	2	-12	$waCH_3 + waCH_{2(e)}$
P16	1072	(+)1075	1069	23	8										$twCH_{2(r)} + waCH_{2(e)}$
P15	1099	(-)1097	1099	17	1	1095	5	-29	1091	20	-9	1094	16	-54	$twCH_{2(r)} + waCH_3$
P14	1117	(+)1112	1117	48	13				1107	15	59	1110	45	72	$twCH_{2(r)} + waCH_3$
P13	1127	(+)1129				1129	93	61							$waCH_3 + waCH_{2(e)}$

P12	1172	(+)1171	1171	143	154	1174	89	-31	1169	296	32	1172	268	8	$twCH_{2(r)} + \nu CO$
P11	1186	(-)1187	1186	165	-145	1191	156	-19	1182	3	9	1182	2	-12	$twCH_{2(r)} + \nu CO$
P10	1217	(-)1218	1220	21	-27	1220	24	-46	1217	18	10	1215	20	-8	$twCH_{2(r)}$
P9		(+)1250										1251	12	39	$twCH_{2(e)}$
P8		(-)1265	1268	1	-13	1258	1	-3	1262	4	23				$twCH_{2(e)}$
P7		(+)1279	1281	3	13				1281	29	12	1282	8	21	$twCH_{2(e)}$
P6	1285	(-)1286	1289	27	-14	1288	13	-11							$waCH_{2(r)}$
P5		(-)1306				1303	3	1	1299	4	-9				$\delta CH + waCH_{2(e)}$
						1311	11	-12				1305	5	-8	$\delta CH + waCH_{2(e)}$
			1326	2	-3				1315	2	6	1320	3	-17	$waCH_{2(r)} + waCH_{2(e)}$
P4	1352	(+)1352	1354	24	4	1355	26	11	1359	39	35	1354	43	29	δCH
P3	1385	(+)1384	1381	2	-1	1379	1	3	1379	4	19	1376	6	21	$\delta CH_{3(symm)}$
			1388	9	31	1384	15	25	1382	2	0	1383	9	11	$waCH_{2(r)} + \delta CH$
P2	1422		1429	9	0	1428	10	0	1429	8	-5	1429	10	-2	$scCH_{2(r)}$
			1438	2	4				1442	3	4				$scCH_{2(e)}$
P1	1461	(-)1461				1454	2	-1				1451	2	-3	$scCH_{2(e)} + scCH_3$
			1462	9	3	1463	14	-10	1461	8	2	1463	3	2	$scCH_3$
			1464	8	-4	1466	1	3	1467	9	1	1469	14	-12	$scCH_{2(r)}$
			1470	10	3	1473	10	-5	1470	10	-2	1471	11	-6	$scCH_3$

[1]B3PW91/ aug-cc-pVTZ level (PCM).[2]The scale factor=0.982 was optimized to maximize the similarity between the experimental and theoretical IR and VCD profiles according to the methodology reported elsewhere [27]; [3]Calculated IR intensities in km/mol; [4]Calculated VCD rotational strengths (Rix10^{-44}) in esu^{2}cm^2; [5] Tentative description based in the visual inspection of the vibrational motions using Gaussview6; Symbols: ν =stretching, ρ =rocking, tw=twisting, wa=wagging, sc= scissoring; δ=deformation; Subscripts: (r)=ring, (e)=ethyl group, (symm)=symmetric.

Again, the vast majority of the bands can be assigned considering solely the presence of the main conformer, the so-called C^{l}_{anti}, which according to calculated Boltzmann's populations (Table 2) represents ca. 50% of the sample composition in CCl_4 solution. Nonetheless, a thorough inspection of the vibrational spectra reveals subtle but consistent evidences of the presence in the medium of the gauche-equatorial conformer. Thus, P23, P13 and P5, which appear at positions that made them not attributable to the main conformer, have been assigned to different vibrational modes of the C^{l}_{gauche} conformer. The P23 band is a shoulder in the IR spectrum at 944 cm^{-1} with a clear positive counterpart in the VCD spectrum which sign is well predicted by quantum chemical calculations. P13 appears as part of a complex-shaped band that can be assigned to the wagging of the ethyl group in the chain of the C^{l}_{gauche} conformer. Note that the calculated intensity for this band is higher than the one calculated for the normal mode that has been assigned to P14 (attributed to the main conformer), reproducing what is observed in the spectrum. Finally, P5 is a weak negative peak in the VCD spectrum at 1306 cm^{-1}, that is not resolved in the IR spectrum under the shape of a broad band centered at 1286 cm^{-1}, but which position and sign is again correctly predicted by quantum chemical calculations.

Apart from the presence of the two equatorial forms, some evidences reveal the presence of the axial conformers in the medium as well. This is the case of P19, P17 and P9.

As concerns P19, it appears 9 cm^{-1} apart from P18, as the low-frequency crest of a broad band and has been assigned to the C-O stretching mode of the gauche-axial conformer. Note that the calculated intensity for this band is considerably high which may explain its observation even though the predicted amounts of this species in the conformational mixture is low (around 10%, see Table 2). One noteworthy question about the vibrational assignment of this region is that the shape of the P18+P19 band can be justified when considering both the gauche conformers (equatorial and axial) since their C-O stretching modes are predicted in the correct position and with high intensities. Nonetheless, the presence of the negative VCD band at 1030 cm^{-1} can only be explained by the intense negative feature that is expected at this wavenumber for the main conformer (equatorial-anti).

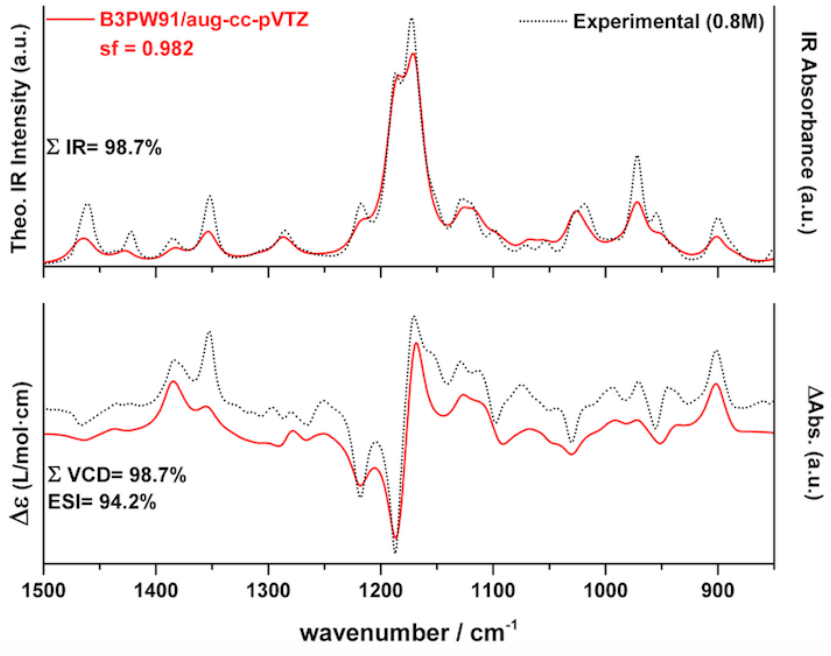

Figure 7. Theoretical-experimental comparison of the IR (above) and VCD (below) of (R)- γ-caprolactone in CCl_4.

In the case of P17, as shown in Table 4, albeit its presence in the IR spectrum would be perfectly explained only by the presence of the equatorial-gauche conformer (C^{I}_{gauche}), the sign of the associated VCD band can only be justified if the presence of axial conformers is contemplated: DFT methods predict strong negative VCD signals associated with the normal modes calculated for both around 1050 cm^{-1} (wagging of the ethyl chain). Finally, P9 is a weak positive band in the VCD spectrum that can be justified if the C^{II}_{gauche} is present. It can be assigned to the twisting of the CH_2 in the ethyl chain, according to its theoretical wavenumber (1251 cm^{-1}) and the strong positive rotational strength calculated for it.

Figure 7 displays the comparison between the IR and VCD spectra of (R)- γ-caprolactone recorded in CCl_4 and those calculated with the PCM: B3PW91/aug-cc-PVTZ method. It is evident that the theoretical method successfully reproduces the experimental observations. As in the case of (R)- γ-valerolactone, the performance of all the methods and basis sets used is good, as revealed by the nice values of the neighbor similarity indices calculated for all of them (see Table 1S and Figure 4S in the ESI) although, again, the B3LYP method offers a slightly poorer performance and the B3PW91 method can be considered the best in terms of statistical parameters.

4. Conclusions

The extensive spectroscopic and computational study carried out for the enantiopure forms of γ-valerolactone and γ-caprolactone in CCl_4 solution has revealed subtle but consistent evidence of conformational mixing in the samples: although the so-called equatorial conformers dominate in both species, the presence of the axial forms, more sterically hindered, has also been evidenced.

The exquisite conformational sensitivity of the VCD technique has proven to be essential in unraveling the conformational landscape of the samples: the main part of the observed vibrational features that allow the discrimination between conformers are present in the VCD spectra.

The complete vibrational assignment that is reported has been assisted by DFT calculations using a whole set of commonly used functionals namely B3LYP, B3PW91, PBE1PBE, ωB97xD and M062x combined with the aug-cc-pVTZ basis set and under the PCM approximation to simulate the solvent.

Although the performance of all methods is comparable, the match between the experimental and theoretical IR and VCD profiles, which has been analyzed in terms of neighborhood similarity (NS) and enantiomeric similarity (ESI) indices, points to the B3PW91 method as the better for both systems, while B3LYP shows a slightly poorer performance. As concerns the size of the basis set (that has also been tested for a group of commonly used basis sets), our results point to the convenience of using basis sets of TZ quality, although no significant improvement (in terms of the values of the statistical similarity indices) is observed when including diffuse functions.

Acknowledgements

We thank to, the "Centro de Instrumentación Científico Técnica" (CICT, University of Jaén) for instrumental facilities and Prof. Herrebout for allowing the use of CompareVOA program.

References

[1] R. Zawirska-Wojtasiak, Chirality and the nature of food authenticity of aroma,

Acta Sci. Pol. Technol. Aliment. 5(1) (2006) 21-36.
[2] a) R. Bentley, The Nose as a Stereochemist. Enantiomers and Odor, Chem. Rev. 106 (2006) 4099-4112; b) J.C. Brookes, A.P. Horsfield, A.M. Stoneham, Odour character differences for enantiomers correlate with molecular flexibility, J. R. Soc. Interface. 6 (2009) 75-86.
[3] Official Journal of the European Union. No 1334/2008. L 354-34
[4] a) A. Mosandl, U. Hener, U. Hagenauer, A. Kustermann, Stereoisomeric Flavor Compounds. 33. Multidimensional gas chromatography direct enantiomer separation of -lactones from fruits, foods, and beverages, J. Agric. Food Chem. 38(3) (1990) 767–771; b) E. Brenna, C. Fuganti, and S. Serra, Enantioselective perception of chiral odorants, Tetrahedron: Asymmetry. 14(1) (2003) 1-42; c) A. Yamamoto, N. Akiba, S. Kodama, A. Matsunaga, K. Kato, H. Nakazawa, Enantiomeric purity determination of malic acid in apple juices by multi-beam circular dichroism detection, J. Chromatogr. A. 928(2) (2001) 139-144.
[5] G. D'Orazio, C. Fanali, M. Asensio-Ramos, S. Fanali, Chiral separations in food analysis, Trends Anal. Chem. 96 (2017) 151–171.
[6] K. H. Engel, G. Takeoka, Importance of Chirality to Flavor Compounds, Washington, DC, 2015.
[7] National Center for Biotechnology Information. PubChem Database. Gamma-Caprolactone. https://pubchem.ncbi.nlm.nih.gov/compound/gamma-Caprolactone, (accessed 24 September 2019).
[8] Chemical Entities of Biological Interest. Gamma-valerolactone https://www.ebi.ac.uk/chebi/chebiOntology.do?chebiId=CHEBI:48569, (accessed 24 September 2019).
[9] A.M.S. Hansen, H.L. Frandsen, A. Fromberg, Authenticity of raspberry flavor in food products using SPME- chiral- GC- MS, Food Sci. Nutr. 4(3) (2016) 348–354.
[10] K.K. Isaacs, W.G. Glen, P. Egeghy, M.R. Goldsmith, L. Smith, D. Vallero, R. Brooks, C.M. Grulke, H. Zkaynak, SHEDS-HT: an integrated probabilistic exposure model for prioritizing exposures to chemicals with near-field and dietary sources, Environ. Sci. Technol. 48(21) (2014) 12750–12759.
[11] C. Barbey, A. Crépin, A. Cirou, A. Budin-Verneuil, N. Orange, M. Feuilloley, D. Faure, Y. Dessaux, J. F. Burini, X. Latour, Catabolic pathway of gamma-caprolactone in the biocontrol agent Rhodococcus erythropolis, J. Proteome Res. 11(1) (2012) 206-216.
[12] W. Xu, Y. Sun, X. Dong, S. Li, H. Wang, J. Xue, Local order and vibrational coupling of the C = O Stretching Mode of γ -Caprolactone in liquid binary mixtures. Sci. Rep. 7 (2017) 12182.
[13] a) P.G. Rodríguez Ortega, M. Montejo, F. Márquez, J.J. López González, DFT-Aided Vibrational Circular Dichroism Spectroscopy study of (-)-S-cotinine, Chem. Phys. Chem. 16(7) 2015 1416-1427; b) P.G. Rodríguez Ortega, M. Montejo, F. Márquez, J.J. López González, Conformational properties of chiral tobacco alkaloids by DFT calculations and Vibrational Circular Dichroism: (−)-S-Anabasine, J. Mol. Graph. Model. 60 (2015) 169-179 c) P.G. Rodríguez Ortega, M. Montejo, J.J. López González, Vibrational Circular Dichroism and theoretical study of the conformational equilibrium in (-)-S-Nicotine, Chem. Phys. Chem. 16(2) (2015) 342–352.
[14] a) D. Rossi, R. Nasti, S. Collina, G. Mazzeo, S. Ghidinelli, G. Longhi, M. Memo, S. Abbate, The role of chirality in a set of key intermediates of pharmaceutical interest, 3-aryl-substituted-γ-butyrolactones, evidenced by chiral HPLC separation and by chiroptical

spectroscopies, J. Pharm. Biomed. Anal. 114 (2017) 41-51; b) G. Mazzeo, A. Cimmino, M. Masi, G. Longhi, L. Maddau, M. Memo, A. Evidente, S. Abbate, Importance and Difficulties in the Use of Chiroptical Methods to Assign the Absolute Configuration of Natural Products: The Case of Phytotoxic Pyrones and Furanones Produced by Diplodia corticol, J. Nat. Prod. 80 (2017) 2406−2415; c) P. Scafato, F. Caprioli, L. Pisani, D. Padula, F. Santoro, G. Mazzeo, S. Abbate, F. Lebon, G. Longhi, Combined use of three forms of chiroptical spectroscopies in the study of the absolute configuration and conformational properties of 3- phenylcyclopentanone, 3-phenylcyclohexanone, and 3-phenylcycloheptanone, Tetrahedron, 69 (2013) 10752-10762; d) E. Giorgio, L. Maddau, E. Spanu, A. Evidente, C. Rosini, Assignment of the absolute configuration of (+)-diplopyrone, the main phytotoxin produced by Diplodia mutila, the pathogen of the cork oak decline, by a nonempirical analysis of its chiroptical properties, J. Org. Chem. 70(2005) 7-13; e) H. Izumi, S. Futamura, L. A. Nafie, R. K. Dukor, Determination of molecular stereochemistry using vibrational circular dichroism spectroscopy: Absolute configuration and solution conformation of 5-formyl-cis,cis-1,3,5-trimethyl-3-hydroxymethylcyclohexane-1-carboxylic acid lactone, Chemical Record 3, (2003) 112-119.

[15] J.M. Dennington, R. Keith, T.A. Millam, “GaussView, Version 6.” Semichem Inc., Shawnee Mission, KS, 2016.

[16] a) T.A. Halgren, R.B. Nachbar, Merck Molecular Force Field. IV. Conformational Energies and Geometries for MMFF94, J. Comput. Chem. 17 (1996) 587–615; b) T.A Halgren, Merck Molecular Force Field. I. Basis, Form, Scope, Parameterization, and Performance of MMFF94, J. Comput. Chem. 17 (1996) 490–519; c) T.A. Halgren, J. Comput. Chem. 17 (1996) 520–552; d) T.A. Halgren, Merck Molecular Force Field. 111. Molecular Geometries and Vibrational Frequencies for MMFF94, J. Comput. Chem. 17 (1996) 553–586; e) T.A. Halgren, Merck molecular force field. V. Extension of MMFF94 using experimental data, additional computational data, and empirical rules, J. Comput. Chem. 17 (1996) 616–641.

[17] a) A.D. Becke, Density-functional thermochemistry. III. The role of exact exchange J. Chem. Phys. 98(7) (1993) 5648–5652; b) C. Lee, W. Yang, R.G. Parr, Development of the Colle-Salvetti correlation-energy formula into a functional of the electron density, Phys. Rev. B. 37(2) (1988) 785–789.

[18] J.P. Perdew, “Quick links,” in Electronic Structure of Solids ‘91, P. Ziesche and H. Eschrig, Eds. Akademie Verlag, Berlin, 1991.

[19] a) J.P. Perdew, K. Burke, M. Ernzerhof, Generalized Gradient Approximation Made Simple, Phys. Rev. Lett. 77(18) (1996) 3865–3868; b) J.P. Perdew, K. Burke, M. Ernzerhof, Generalized Gradient Approximation Made Simple, Erratum: Phys. Rev. Lett 78(8) (1997) 1396; c) C. Adamo, V. Barone, Toward reliable density functional methods without adjustable parameters: The PBE0 model, J. Chem. Phys. 110(13) (1999) 6158–6170.

[20] J.D. Chai, M. Head-Gordon, Long-range corrected hybrid density functionals with damped atom–atom dispersion corrections, Phys. Chem. Chem. Phys. 10(44) (2008) 6615-6620.

[21] Y. Zhao, D. G. Truhlar, The M06 suite of density functionals for main group thermochemistry, thermochemical kinetics, noncovalent interactions, excited states, and transition elements: two new functionals and systematic testing of four M06-class functionals and 12 other functionals, Theor. Chem. 120 (2008) 215–241.

[22] M.J. Frisch, J.A. Pople, J.S. Binkley, Self-consistent molecular orbital methods 25. Supplementary functions for Gaussian basis sets, J. Chem. Phys. 80 (7) (1984) 3265-3269.
[23] N. Godbout, D. R. Salahub, J. Andzelm, and E. Wimmer, Optimization of Gaussian-type basis sets for local spin density functional calculations. Part I. Boron through neon, optimization technique and validation, Can. J. Chem., 70 (1992) 560-71.
[24] a) R.A. Kendall, T.H. Dunning, R.J. Harrison, Electron affinities of the first-row atoms revisited. Systematic basis sets and wave functions, J. Chem. Phys. 96(9) (1992) 6796-6806; b) D E. Woon, T.H, Dunning, Gaussian basis sets for use in correlated molecular calculations. III. The atoms aluminum through argon, J. Chem. Phys. 98(2) (1993) 1358-1371.
[25] G. Scalmani, M.J. Frisch, Continuous surface charge polarizable continuum models of solvation. I. General formalism, J. Chem. Phys. 132(11) (2010) 114110-114124.
[26] D.J. Frisch, M.J. Trucks, G.W. Schlegel, H.B. Scuseria, G.E. Robb, M.A. Cheeseman, J. R. Scalmani, G. Barone, V. Petersson, G. A. Nakatsuji, H.Li, X. Caricato, M. Marenich, A. V. Bloino, J. Janesko, B. G. Gomperts, R. Mennucci, B. Hratch et al., "Gaussian 16, Revision C.01." Gaussian, Inc., Wallingford CT, 2016.
[27] a) J. Vandenbussche, P. Bultinck, A.K. Przybyl, W.A. Herrebout, Statistical validation of absolute configuration assignment in vibrational optical activity, J. Chem. Theory Comput. 9(12) (2013) 5504-5512. b) E. Debie, E. De Gussem, R.K. Dukor, W.A. Herrebout, L.A. Nafie, P. Bultinck, Confidence level algorithm for the determination of absolute configuration using vibrational circular dichroism or Raman optical activity, Chem. Phys. Chem. 1(8) (2011) 1542-1549.
[28] a) C. Merten, T. P. Golub, N. M. Kreienborg, Absolute Configurations of Synthetic Molecular Scaffolds fromVibrational CD Spectroscopy, J. Org. Chem. 84 (2019) 8797–8814 (and references therein); b) P. J. Stephens, F. J. Devlin, J-J. Pan, The determination of the absolute configurations of chiral molecules using vibrational circular dichroism (VCD) spectroscopy, Chirality, 20 (2008) 643-663 (and references therein).

a)

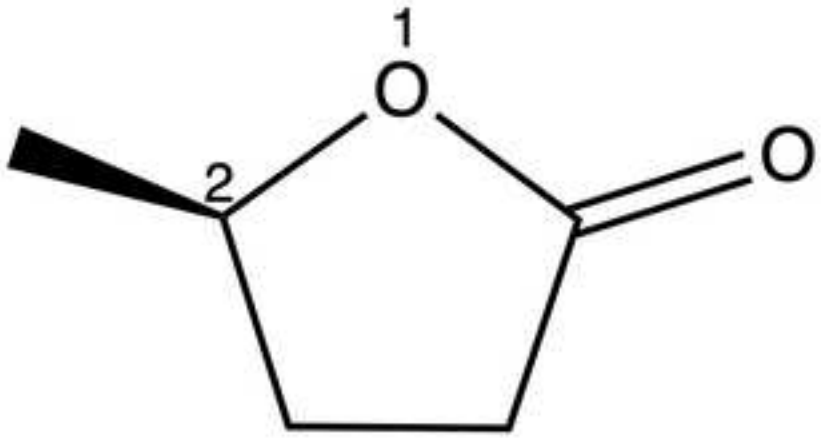

(*R*)-5-methyldihydrofuran-2(3*H*)-one

b)

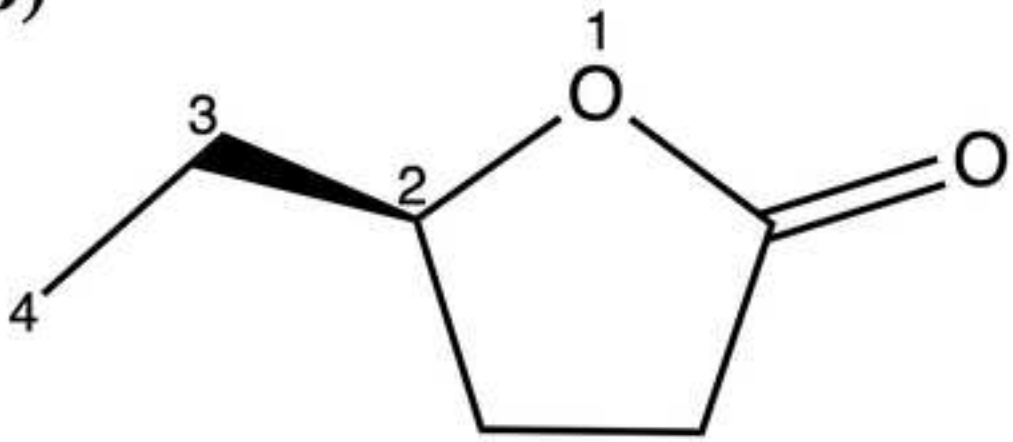

(R)-5-ethyldihydrofuran-2(3H)-one

Figure 3

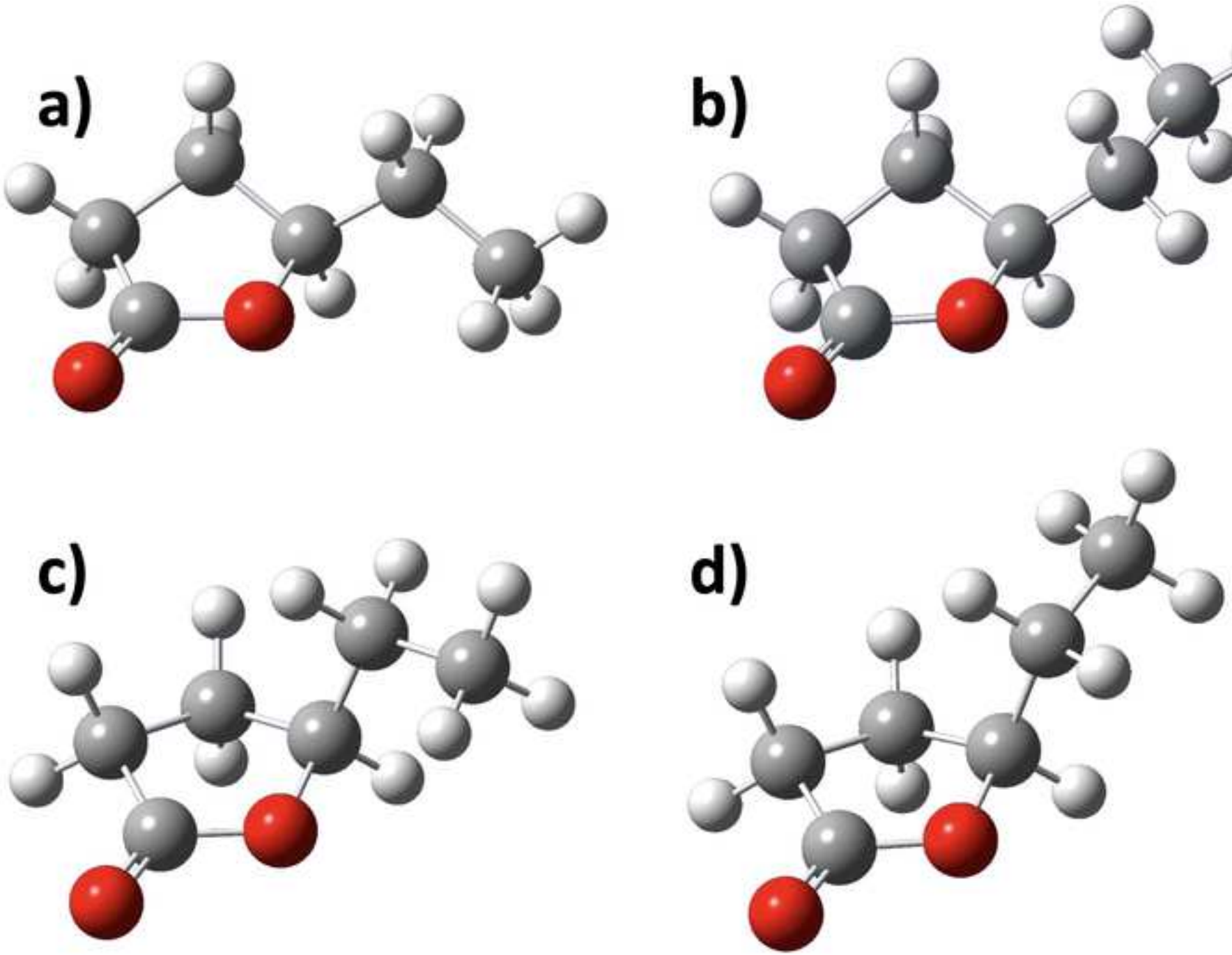

Figure 4

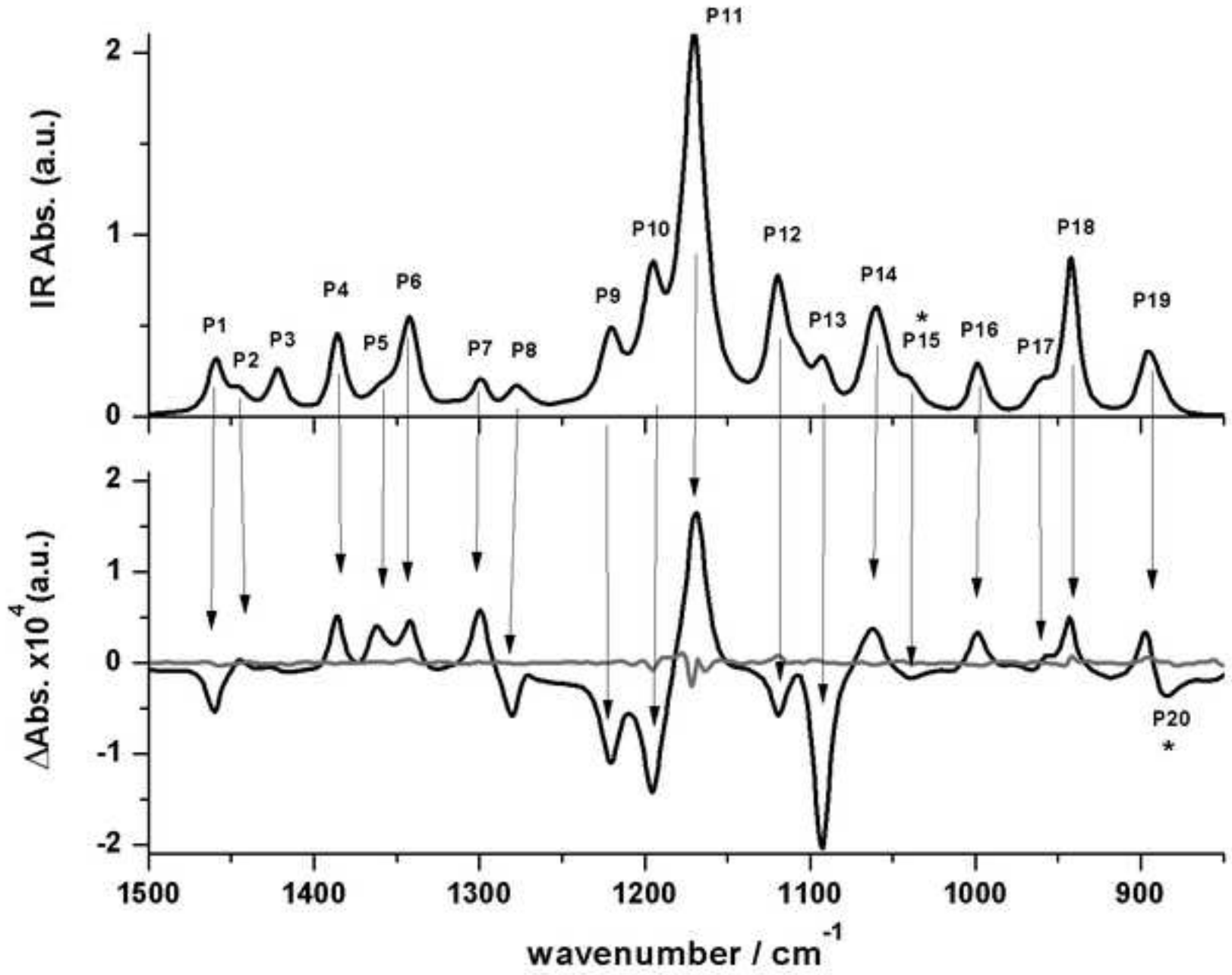

Figure 6

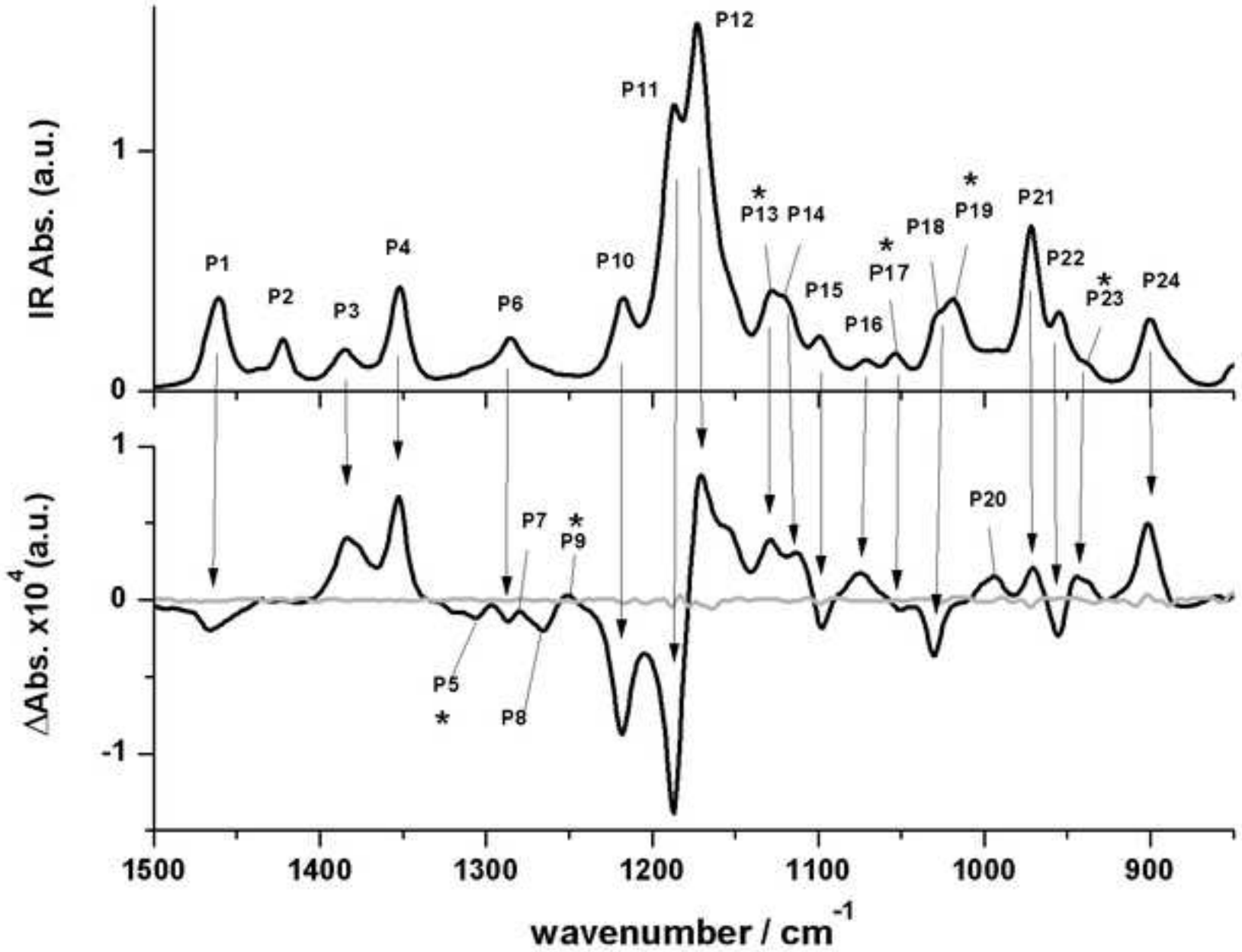

Author contributions:

PGRO and MMG: Conceptualization, Formal analysis, Supervision, Validation, Writing – review & editing. **MSV and RCJ:** Data curation; Methodology.

Declaration of interests

☒ The authors declare that they have no known competing financial interests or personal relationships that could have appeared to influence the work reported in this paper.

☐The authors declare the following financial interests/personal relationships which may be considered as potential competing interests: